Ex vivo porcine model for eye, eyelid, and orbit movement analysis of 4-mm ferromagnetic foreign bodies in MRI

Marwane Ghemame, C. Cathelineau, Béatrice Carsin-Nicol, Pierre-Antoine Eliat, Hervé Saint-Jalmes, Jean-Christophe Ferré, Frédéric Mouriaux

HAL Id: hal-03331703
https://hal.science/hal-03331703

Ex vivo porcine model for eye, eyelid, and orbit movements analysis of 4-mm ferromagnetic foreign bodies in MRI

Ghemame, M.[1+], Cathelineau, C.[2,+], Carsin-Nicol, B.[2], Eliat, P-A.[3], Saint-Jalmes, H.[4], Ferré, J-C.[2,5,A], and Mouriaux, F.[1,6,A]

[1] Rennes University Hospital, Department of Ophthalmology, F-35000 Rennes, France

[2] Rennes University Hospital, Department of Neuroradiology, F-35033 Rennes, France

[3] University of Rennes, CNRS, Inserm, BIOSIT- UMS 3480, US_S 018, F-35000 Rennes, France

[4] University of Rennes, Rennes University Hospital, CLCC Eugène Marquis, Inserm, LTSI - UMR 1099, F-35000 Rennes, France

[5] University of Rennes, Rennes University Hospital, Inria, CNRS, INSERM, IRISA, Empenn ERL U-1228, F-35000 Rennes, France

[6] University of Rennes, Rennes, INSERM, UMR 1241, Nutrition, Métabolismes et Cancer (NuMeCan)

Ghemame, M. ORCID: 0000-0002-8057-1625

Cathelineau, C. ORCID: 0000-0001-6644-6142

Carsin-Nicol, B. ORCID: 0000-0002-3791-2615

Eliat, P-A. ORCID: 0000-0002-8082-4477

Ferré, J-C. ORCID: 0000-0003-3911-1800

Mouriaux, F. ORCID: 0000-0001-9183-4235

*corresponding author: marwane.ghemame@chu-rennes.fr

+ GM and CC contributed equally to the work presented here and should therefore be regarded as equivalent senior authors.

A JCF and FM contributed equally to the work presented here and should therefore be regarded as equivalent senior authors.

Key messages
MRI is described as prohibited in case of ocular ferromagnetic foreign bodies.

We confirm that MRI is contraindicated for patients with choroidal and intravitreous ferromagnetic foreign bodies.

Nevertheless, we showed that MRI should not be contraindicated for patients with eyelids ferromagnetic foreign bodies.

Abstract

Purpose: Ferromagnetic foreign bodies (FFB) present during magnetic resonance imaging (MRI) explorations can lead to tissue injury due to movement, especially in and around the eyes. Ferromagnetic foreign bodies located in the intraocular area, eyelids, and orbit are thus prohibited from undergoing MRI. The aim of the study was to analyze movement of 4-mm ferromagnetic foreign bodies in MRI in eye, eyelid, and orbit using computer tomography (CT scan).

Method: We developed a porcine model using 12 quarters of fresh porcine heads. Each porcine head included one whole orbit with the ocular globe, orbital fat, muscles, and eyelids. 4-mm FFB were implanted in the eye within two days post-slaughter and images were acquired within five days post-slaughter. 4-mm FFB movement was analyzed after 1.5 Tesla (T) MRI. Four locations were tested: intravitreous, suprachoroidal, intraorbital fat, and intrapalpebral. Movement analysis was assessed using computed tomography (CT scan).

Results: The intravitreous ferromagnetic ball moved 14.0±8.8 mm ($p<0.01$), the suprachoroidal ball moved 16.8±5.4 mm ($p<0.01$), the intraorbital fat ball moved 5.8±0.9 mm ($p>0.05$), and the intrapalpebral ball moved 2.0±0.4 mm ($p>0.05$).

Conclusion: The ex vivo porcine model was able to study FFB movement. The 4-mm ferromagnetic balls moved in intravitreous and in suprachoroidal locations after MRI.

Funding None

Conflicts of interest/Competing interests None

Availability of data and material Not applicable

Code availability Not applicable

Authors' contributions
+ GM and CC contributed equally to the work presented here and should therefore be regarded as equivalent senior authors.

A JCF and FM contributed equally to the work presented here and should therefore be regarded as equivalent senior authors.

Introduction

Magnetic Resonance Imaging (MRI) is a powerful tool used to study anatomy and diagnose diseases in medical practice. Most scanners installed for general diagnostic purposes are 1.5 T in strength [1]. This strong magnetic field is responsible for adverse events [2]. Patients who have a ferromagnetic foreign body cannot benefit from MRI exploration since the magnetic field may induce a torque effect and local heating. Thus, MRI has been described as contraindicated if intraocular, eyelid, or orbit ferromagnetic foreign bodies (FFB) are suspected. Potential injury of the globe and/or orbit occurs due to foreign body displacement.

Few scientific papers have been published on FFB movement due to MRI using animal models. The first study was conducted by Lagouros *et al.* [3] in 1987 on eight pigmented rabbit eyes under anesthesia. All animals underwent MRI followed by indirect ophthalmoscopy. Because of retinal injuries due to intravitreous FFB, they concluded that 1.5 T MRI was contraindicated for eye trauma with suspected FFB. However, no mention of foreign body size was described. In 1988, Williams *et al.* [4] placed steel fragments in the cornea, sclera, vitreous, fornix conjunctiva, and orbits of eighteen New Zealand white rabbit eyes under anesthesia. Movement was detected using X-rays and indirect ophthalmoscopy. They concluded that small metal fragments are unaffected by 2.0 T MRI scans, whereas only intravitreous larger-sized foreign bodies ($3x1x1mm^3$) moved in a magnetic field, but with no evidence of clinical ocular damage. In 1989, Williamson *et al.* [5] used twenty bovine eyes and 10 to 20-mm long steel needles in vitreous and the suprachoroidal space. These bovine eyes underwent 0.08 T MRI. After anatomic dissection, no ocular damage due to FFB movement was observed. In 1992, Gunenc *et al.* [6] implanted nine fresh bovine eyes with various sizes of magnetic foreign bodies using a CT scan to characterize the foreign bodies. Then, they dissected bovine eyes to detect movement after 1.0 T MRI and concluded that iron, chromium, and solder foreign bodies had changed their position in these bovine eyes. A more recent study was conducted by Cullen *et al.* [7] in 2002 using twenty rabbits under anesthesia with 1.5 T MRI. They used a 3 mm × 0.72 mm section of a stylet from a 22-gauge spinal needle located in the vitreous. They concluded that magnetic field exposure did not induce ocular injury, but only vitreous pathologic changes using computed tomography (CT scan). These contradictory findings led us to develop an ex

vivo animal model to study how FFB would move in vitreous, eyelid, suprachoroidal, and orbital fat tissues after passing through a 1.5 T MRI scanner, using CT to analyze FFB movement.

Materials and Methods

Animals

Twelve quarters of fresh porcine heads were obtained from a butcher donation less than three days after slaughter. For the purpose of simplification, "porcine head" means each quarter of a fresh porcine head used. Each porcine head included one whole orbit with a globe, orbital fat, muscles, and eyelids. FFB were implanted within two days and images were acquired within five days post-slaughter. Porcine heads were conserved in a refrigerator between manipulations without freezing.

Steel ball (FFB) implantation

We used calibrated 4-mm FFB steel balls that included at least 98% iron (Figure 1) [8]. Iron is a ferromagnetic metal responsible for MRI artefacts. All our MRI images showed magnetic susceptibility artefacts where foreign bodies were located, especially on echo planar (gradient-echo) sequences, which proved that all foreign bodies used in this study were metallic with a ferrous composition (personal communication).

Figure 1: 4-mm steel ball

One FFB was surgically implanted per porcine head in each of four locations: suprachoroidal (SC), intraorbital fat (IO), intrapalpebral (IP), or intravitreous (IV). FFB were implanted in triplicate for each location (twelve porcine heads in total). For each porcine head, Vicryl 4-0 traction wire was pulled through the upper and lower eyelids, then the nictitating membrane was removed, followed by external cantholysis. For all dissections a standard 15° ophthalmologic blade was used (Figure 2).

Figure 2: FFB implantation

A: eyelid traction wire, B: removal of nictitating membrane, C: scleral flap creation,

D: suprachoroidal implantation, E: scleral flap stitching, F: 3 stitches with Vicryl 6-0,

G: intrapalpebral implantation, H: eyelid stitching, I: intravitreous implantation

SC-FFB implantation: a bridle suture in the superior cornea with Vicryl 4-0 was carried out to depress the eye. A superior peritotomy was performed for the creation of a triangular scleral flap 3 mm behind the limbus, without choroid injury and/or vitreous leakage. An FFB was then implanted in the SC location. The scleral flap was stitched with Vicryl 6-0. Finally, the eyelid and corneal traction wires were cut.

IP-FFB implantation: an incision in the middle of the lower eyelid between the tarsus and the conjunctiva was performed. The FFB was then placed into the orbicularis. After foreign body implantation, the tarsus and conjunctiva were stitched. Finally, eyelids were stitched together to avoid movement.

IO-FFB implantation: Vicryl 4-0 was used to stitch the superior cornea to depress the eye. A fornix conjunctival incision was made inferiorly. An FFB was implanted deep in the orbital fat, under the globe. The conjunctiva and tenon were stitched with Vicryl 6-0. Finally, corneal traction wire was removed.

IV-FFB implantation: a bridle suture in the superior cornea using Vicryl 4-0 was performed, depressing the eye. After a superior peritotomy, a scleral pars plana incision was made 3 mm behind the limbus. An FFB was placed into the vitreous, and the sclera was stitched with Vicryl 6-0. Finally, eyelid and corneal traction wires were removed.

Airtight container and scanners

Porcine heads implanted with FFB were positioned onto a fixed plywood surface and placed into an airtight PVC 17 cm long x 12.5 cm diameter container to facilitate manipulation and positioning-repositioning. Porcine heads were always oriented in the same way: snout in front, eye facing up, surrounded by large compresses to avoid movement of the porcine head. Two saline fiducial markers (saline pipettes) were placed under the flat surface in polyurethane foam to check the position during the MRI scan. Containers were marked with a cross on the "front" and the "back", with a straight line on the top to facilitating positioning-repositioning inside the scanners (Figure 3). For CT scans, pads were wedged under the airtight container, all of which was carefully positioned using the CT scanner laser. For MRI, the airtight container was positioned at the center of the head coil, wedged with pads, and its orientation was the same as in the CT scanner.

Figure 3: Airtight container

PVC box with flat plywood surface fixed with glue and polyurethane foam. The box was marked with "front", "back", and a straight line on the top, and a cross in the front.

CT studies were performed using a 64-detector row Aquilion PRIME scanner (Canon Medical Systems, Otawara, Japan) with the following parameters: 120 kV with automatic mAs modulation, 0.75-second rotation time, 0.5-mm collimation and 0.625-mm spiral pitch factor. Image reconstruction was performed with a hard reconstruction kernel (FC35), resulting in 244 slices with a 0.8 mm gap, an image matrix of 512x512 with a voxel size of 0.3x0.3 x 1 mm. MR scanning was performed on a 1.5T scanner (Optima MR450w General Electric Medical Systems Milwaukee, Wisconsin), using a 24-channel head coil. Conventional MRI sequences, including spin-echo FLAIR and gradient-echo acquisitions as well as diffusion echo planar imaging, were performed to mimic a typical patient examination with a total acquisition time of 20 min.

CT and MRI scanners were located in the same hospital, separated by a 5-min walk. The duration of the process lasted less than 1.5 hours. All CT and MR images were transferred to the PACS TELEMIS® TM (Version 4.80, Louvain-la-Neuve, Belgium). The acquisitions protocol was: CT scan 1 for FFB confirmation of location; 5-min walk with stairs; CT scan 2 to assess the potential displacement due to handling of the head between examinations; MRI scan in which the container was carefully introduced into and removed from the magnetic field core in the same way and at the same speed; CT scan 3 to measure steel ball displacement after the MRI scan. FFB displacement was measured using CT scan 2 and CT scan 1 to assess potential displacement due to handling of the head between examinations. CT scan 3 and CT scan 2 were used to measure steel ball displacement after the MRI (Figure 4). All measurements were assessed using ITK-SNAP® open source software on PC (Version 3.8.0, Pennsylvania, USA) [9]. A 3D manual reconstruction was done comparing volumes using orbital bones, ocular muscles, and the sinus as anatomical landmarks. Then, ball center positions measured on CT images were used to determine mean ball displacement in three dimensions derived from the Pythagorean theorem.

Comparisons of displacement in the different location groups (MRI vs the 5-min walk) was performed by a parametric Student's test.

Figure 4: Study scheme

Results

The 4-mm steel balls were successfully surgically implanted in twelve porcine heads (PX: porcine head number X) in the four different locations. These locations were all confirmed on CT scan 1.

MRI scan artefacts

MRI images showed susceptibility magnetic artefact as a large magnetic field distortion.

Sub millimetric movement of steel balls after a 5-min-walk test

To assess whether manipulation of the airtight container may induce movement, FFB displacement was analyzed before and after a 5-min-walk test with stairs. FFB displacement was measured using CT scan 2 and CT scan 1 to assess the potential displacement due to the handling of heads between examinations. The mean (±SD) displacement was 0.73±0.3 mm after the 5-minute-walk test. Displacements all measured less than one millimeter (Table 1 and Figure 5).

Figure 5: steel balls displacements

A: CT scan 1 and 2 before registration: the two scans are not "matched"

B: CT scan 1 and 2 after registration based on bones structures

Top: coronal plane. Middle: axial plane. Bottom: sagittal plane

C: CT scan 2 and 3: SC-FFB movement in coronal plane (porcine head P1)

D: CT scan 2 and 3: IV-FFB movement in coronal plane (porcine head P4)

Using a filter: FFB was pink before MRI scan and grey after MRI scan

The ex vivo model is able to detect steel ball movement induced by MRI examination

FFB displacement due to MRI was assessed comparing CT scan 3 to CT scan 2. Mean steel ball displacements are illustrated on Figure 5. Displacement was different depending on location: IO-FFB and IP-FFP displacements were less than 6 mm, whereas SC-FFB and IV-FFB were more than 14 mm (Table 2). Considering the minimal movement induced by manipulation of

the airtight container, Student's test showed significant movement for SC-FFB and IV-FFB ($p<0.01$). However, IO-FFB and IP-FFB did not show any significant movement ($p>0.05$).

Discussion

A few months ago, we observed a signal distortion in the eyelid of a patient after an orbital MRI exploration. An X-ray image showed the presence of a metallic foreign body. The patient was unaware of this foreign body and no ocular lesions were observed. We therefore considered that the foreign body in our patient had not moved. Nevertheless, this observation cannot be generalized: this patient may have benefited from favorable circumstances as healing process. As described before, few scientific papers have been published on FFB movement due to MRI using animal models, and results are contradictory. However, a few case reports have been published, and results are contradictory as well. In 2014, Lawrence *et al.* [10] reported a case of hyphema after MRI in a 47-year-old man with an undetected ferromagnetic metallic intraocular foreign body who underwent an elective MR examinations for chronic back pain. In 2017, Platt *et al.* [11] reported a case of a 12-years-old boy with a retinal metallic foreign body who underwent an MRI without complications. To our knowledge, our study is the first to explore four different locations of 4-mm foreign bodies including the palpebral area, and also the first using CT scans to assess movement after MRI.

Rabbit heads have been used in other studies [3,4]. We first experimented with this model, but encountered two main issues leading us to change it. First, the small size of a rabbit's head makes it difficult to implant a large-sized FFB. Second, the mismatch between small rabbit' heads and large FFB decreases reproducibility of measurements. Moreover, rabbit heads have so little soft tissue that the MRI signal was too limited to start the scanning process. In contrast, the porcine model is closer to human anatomy and is often used in vision research, such as retinal [12], glaucoma [13], and cataract surgery studies [14]. Interestingly for our study, the sclera is very similar, with 70% water [15], and with the vitreous having the same composition of collagen and hyaluronate sodium [16] accounting for 80% of the volume of the eyeball. Thus, we used the "natural" orbital fat for preserving tissue anatomy, in contrast to the study of Gor *et al.* [17] who placed porcine eyes surrounded by vegetable fat in human skulls to simulate orbital fat in in-vivo conditions. Moreover, in our model, porcine heads were implanted within less than 5 days

after slaughter and were stored in a refrigerator to avoid putrefaction. Therefore, ocular muscles, sinuses, and orbital bones were clearly seen, allowing reproducible implantations and locations in the four areas (intraorbital fat: IO-FFB, intrapalpebral: IP-FFB, intravitreous: IV-FFB and suprachoroidal: SC-FFB), and facilitated imaging measurements. Nevertheless, dead tissues have no inflammation or sclerotic reactions, as occurs in in vivo models when a metallic body is present for a long time.

The 5-min-walk test was necessary before interpreting displacement. The displacement of porcine heads between CT and MRI could theoretically induce movement. For reproducibility, orbits were always oriented in the same way in the MRI device by using an airtight container to avoid rotation and to facilitate recalibration of the software. We demonstrated that CT scans before and after the 5-min-walk test did not show movement exceeding 1.5 mm. Thus, we can conclude that movement detected after the MRI scan was mainly due to the magnetic field. In contrast to Cullen *et al*, who used one size of foreign body in one location in rabbit eyes, we used 4-mm FFB in four locations. But the exact amount of rotation could not be measured accurately in the coronal, axial, and sagittal planes due to loss of signal induced by metal artefacts on MR images (personal communication).

We observed that movement was most significant in suprachoroidal (mean 16.8 mm) and intravitreous (mean 14 mm) locations. However, we noted that one steel ball in the vitreous location moved only 3.8 mm in one porcine head, maybe by vitreous condensation after death. Our results confirmed the high risk of FFB displacement during MRI scans in suprachoroidal and intravitreous locations. For intraorbital FFB, movement was less marked, with a mean of 5.8 mm. However, intraorbital fat movement in MRI probably occurs less often in clinical practice because of tissue fibrosis that encapsulates foreign bodies in granulomas. For palpebral locations, movement was not significant. In fact, as in the orbit, ex vivo studies do not preclude the consideration of fibrosis that can occur in contact with foreign bodies in "real" life. Artefacts can imped MRI scans analysis. However, 4-mm steel ball prevent us only to analyze the orbit, but not the brain. Thus, patients with IP-FFB who were initially not eligible for MRI may benefit from a brain analysis.

Not monitoring local heating is a limit of our study. Induced heating during MRI procedures has been tested in a review by Shellock et al. [18]. The authors concluded that only minor temperature changes occurred when MRI procedure involved metallic implants.

These results of reduced movement in eyelids confirms our personal cases of IP-FFB without complications after MRI. Should we consider not prohibiting MRI with IP-FFB? The number of porcine heads included in our study is not sufficient to answer this question clearly. The next step would be to include more cases and different sizes of FFB.

COMPLIANCE WITH ETHICAL STANDARD

REFERENCES

1.   Detournay. B, Courouve. L (2017). *Les insuffisances en matière d'équipement d'imagerie médicale en France*.
http://www.sfrnet.org/rc/org/sfrnet/htm/Article/2015/20150625-083932-499/src/htm_fullText/fr/2015-014%20ISA%20IRM%20Rapport%2013-05-15.pdf

2.   Schenck, J. F. (2000) Safety of Strong, Static Magnetic Fields. *Journal of Magnetic Resonance Imaging* 12, 2–19.

3.   Lagouros, P. A. *et al.* (1987) Magnetic Resonance Imaging and Intraocular Foreign Bodies. *Archives of Ophthalmology* 105, 551–553

4.   Williams, S., Char, D. H., Dillon, W. P., Lincoff, N. & Moseley, M. (1988) Ferrous Intraocular Foreign Bodies and Magnetic Resonance Imaging. *American Journal of Ophthalmology* 105, 398–401

5.   Williamson, T. H., Smith, F. W. & Forrester, J. V. (1989) Magnetic resonance imaging of intraocular foreign bodies. *British Journal of Ophthalmology* 73, 555–558

6.   Gunenc, U., Ahmet, M., Suleyman, K. & Tugrul, P. (1992) Magnetic resonance imaging and computed tomography in the detection and localization of intra ocular foreign bodies. *Documentia Ophtalmologica* 81, 369–378 DOI 10.1007/BF00169098

7.   Cullen, C., Kendall, E., Cui, J., Colleaux, K. & Grahn, B. (2002) The effects of exposure to a 1.5-tesla magnetic field on intravitreous metallic foreign bodies in rabbits. *Graefe's Arch Clin Exp Ophthalmol* 240, 393–402

8.   Duratool (2014). 450 piece steel Ball Assortment *V1.0* 2057
https://cpc.farnell.com/duratool/d01897/steel-ball-assortment-450pc/dp/FN02654#anchorTechnicalDOCS

9.   Yushkevich, P. A. *et al.* (2006) User-guided 3D active contour segmentation of anatomical structures: Significantly improved efficiency and reliability. *NeuroImage* 31, 1116–1128

10.   Lawrence, D. A., Lipman, A. T., Gupta, S. K. & Nacey, N. C. (2015) Undetected intraocular metallic foreign body causing hyphema in a patient undergoing MRI: a rare occurrence demonstrating the limitations of pre-MRI safety screening. *Magnetic Resonance Imaging* 33, 358–361

11.   Platt, A. S., Wajda, B. G., Ingram, A. D., Wei, X.-C. & Ells, A. L. (2017) Metallic intraocular foreign body as detected by magnetic resonance imaging without complications–A case report. *American Journal of Ophthalmology Case Reports* 7, 76–79

12.   Fernandez-Bueno, I., Pastor, J. C., Gayoso, M. & Alcalde, I. (2008) Müller and macrophage-like cell interactions in an organotypic culture of porcine neuroretina. *Molecular Vision* 14:2148-2156,

13.   Ruiz-Ederra, J. *et al.* (2005) The pig eye as a novel model of glaucoma. *Experimental Eye Research* 81, 561–569

14.   Nishi, O., Nishi, K., Nishi, Y. & Chang, S. (2008) Capsular bag refilling using a new accommodating intraocular lens: *Journal of Cataract & Refractive Surgery* 34, 302–309

15.   Olsen, T. W., Sanderson, S., Feng, X. & Hubbard, W. C. (August2002) Porcine Sclera: Thickness and Surface Area. *IOVS Investigative Ophthalmology & Visual Science* 43, 4 PMID: 12147580

16.   Swindle, K. E., Hamilton, P. D. & Ravi, N. (2008) *In situ* formation of hydrogels as vitreous substitutes: Viscoelastic comparison to porcine vitreous. *J. Biomed. Mater. Res.* 87A, 656–665

17.   Gor, D. M., Kirsch, C. F., Leen, J., Turbin, R. & Von Hagen, S. (2001) Radiologic Differentiation of Intraocular Glass: Evaluation of Imaging Techniques, Glass Types, Size, and Effect of Intraocular Hemorrhage. *American Journal of Roentgenology* 177, 1199–1203

18.   Shellock, F. G. (2000) Radiofrequency energy-induced heating during MR procedures: a review. *J Magn Reson Imaging* 12, 30–36

Figure 1: 4-mm steel ball

Figure 2: FFB implantation

A: eyelid traction wire, B: removal of nictitating membrane, C: scleral flap creation,
D: suprachoroidal implantation, E: scleral flap stitching, F: 3 stitches with Vicryl 6-0,
G: intrapalpebral implantation, H: eyelid stitching, I: intravitreous implantation

Figure 3: Airtight container
PVC box with flat plywood surface fixed with glue and polyurethane foam. The box was
marked with "front", "back", and a straight line on the top, and a cross in the front.

Figure 4: Study scheme

Figure 5:

A: CT scan 1 and 2 before registration: the two scans are not "matched"
B: CT scan 1 and 2 after registration based on bones structures
Top: coronal plane. Middle: axial plane. Bottom: sagittal plane

C: CT scan 2 and 3: SC-FFB movement in coronal plane (porcine head P1)
D: CT scan 2 and 3: IV-FFB movement in coronal plane (porcine head P4)
Using a filter: FFB was pink before MRI scan and grey after MRI scan.
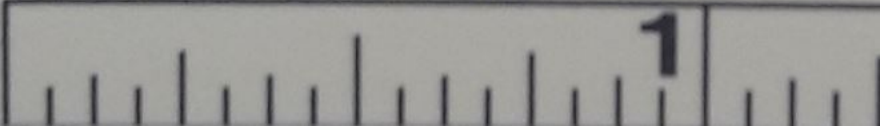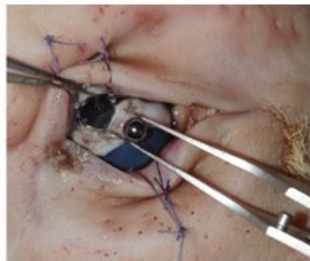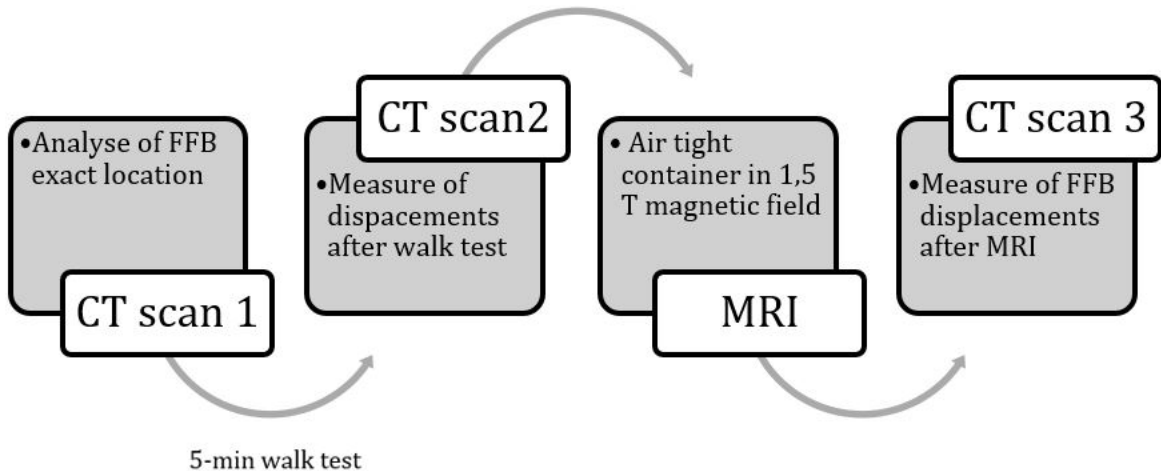
METRIC
INCHES **Devon**® OR Produ

1

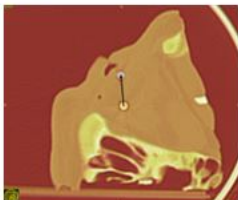| A	B	C
D	E	F
G	H	I

CT scan 1
- Analyse of FFB exact location

CT scan2
- Measure of dispacements after walk test

MRI
- Air tight container in 1,5 T magnetic field

CT scan 3
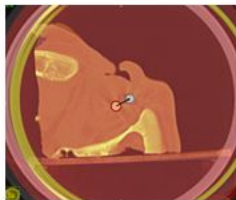- Measure of FFB displacements after MRI

5-min walk test

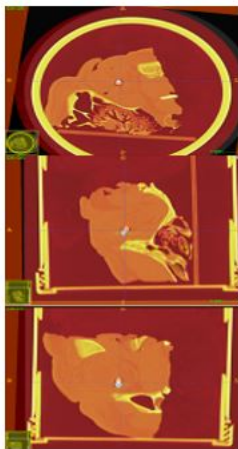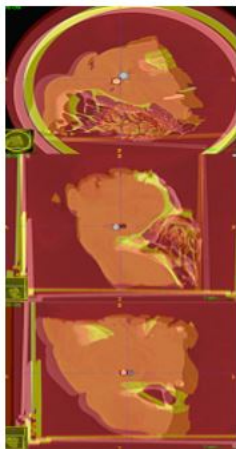| A	B
C	D

Table 1: FFB displacements in millimeters after 5 minutes walk's test

Location	Porcine head	Displacement (mm)	Mean value ± SD (mm)
SC-FFB	P1	0.7	
	P5	0.8	0.7 ± 0.06
	P9	0.7	
IO-FFB	P2	0.6	
	P6	0.7	0.6 ± 0.06
	P10	0.6	
IP-FFB	P3	0.5	
	P7	1.5	1.0 ± 0.5
	P11	1.0	
IV-FFB	P4	0.6	
	P8	0.4	0,5 ± 0.1
	P12	0.5	

Legend: PX: porcine head number X / suprachoroïdal foreign body: SC-FFB / intraorbital fat foreign body: IO-FFB / intrapalpebral foreign body: IP-FFB / intravitreous foreign body: IV-FFB

Table 2: Steel balls displacements induced by MRI examination

Location	Porcine head	Displacement (mm)	Mean value ± SD (mm)
SC-FFB	P1	11.4	16.8* ± 5.4
	P5	16.8	
	P9	22.1	
IO-FFB	P2	4.8	5.8 ± 0.9
	P6	5.9	
	P10	6.6	
IP-FFB	P3	2.2	2.0 ± 0.4
	P7	1.5	
	P11	2.3	
IV-FFB	P4	19.2	14.0* ± 8.8
	P8	3.8	
	P12	19.0	

Legend: PX: porcine head number X / suprachoroïdal foreign body: SC-FFB / intraorbital fat foreign body: IO-FFB / intrapalpebral foreign body: IP-FFB / intravitreous foreign body: IV-FFB
Significant p value < 0.01 are shown with *.